An Anion Antiporter Model of Prestin, the Outer Hair Cell Motor Protein

Daniella Muallem and Jonathan Ashmore
Department of Physiology, University College London, London, United Kingdom

ABSTRACT Cochlear amplification in mammalian hearing relies on an active mechanical feedback process generated by outer hair cells, driven by a protein, prestin (SLC26A5), in the lateral membrane. We have used kinetic models to understand the mechanism by which prestin might function. We show that the two previous hypotheses of prestin, which assume prestin cannot operate as a transporter, are insufficient to explain previously published data. We propose an alternative model of prestin as an electrogenic anion exchanger, exchanging one Cl^- ion for one divalent or two monovalent anions. This model can reproduce the key aspects of previous experimental observations. The experimentally observed charge movements are produced by the translocation of one Cl^- ion combined with intrinsic positively charged residues, while the transport of the counteranion is electroneutral. We tested the model with measurements of the Cl^- dependence of charge movement, using SO_4^{2-} to replace Cl^-. The data was compatible with the predictions of the model, suggesting that prestin does indeed function as a transporter.

INTRODUCTION

Outer hair cells (OHCs) are one class of sensory cells of the inner ear and play an important role in enhancing the sensitivity and frequency selectivity of mammalian hearing (1). Prestin (SLC26A5) is specifically expressed in the basolateral membrane of OHCs (2) and is believed to underlie voltage-dependent OHC length changes, known as electromotility (3). This is the likely basis for cochlear amplification. The mechanical response is correlated with gating-charge movements, similar to those observed for ion channels, giving rise to a voltage-dependent nonlinear component of membrane capacitance (NLC) (4,5). The bell-shaped NLC can be described by the derivative of a two-state Boltzmann function, given by

$$NLC(V) = \frac{\beta Q_{\max} e^{-\beta(V-V_o)}}{(1+e^{-\beta(V-V_o)})^2}, \quad (1)$$

where $\beta = (ze_o\delta/k_BT)$, $Q_{\max}$ is the maximum charge transferred across the membrane, V_o is the potential at half-maximal charge transfer; z is number of elementary charges, e_o, displaced across a fraction, δ, of the membrane dielectric; k_B is Boltzmann's constant and T is the absolute temperature. β depends on both the magnitude of the gating charge and the distance moved by it. Experimental data gives values for β of $\sim 0.03\ mV^{-1}$ (5,6), which corresponds to one elementary charge crossing ~80% of the membrane field. It has been proposed that this charge movement is coupled with a conformational change of prestin, producing a small change in protein area that is translated into a change in cell length due to the high density of proteins in the membrane (7,8).

Prestin belongs to the recently identified SLC26 family of anion transporters. These transporters are structurally different from the classical SLC4 family of bicarbonate (HCO_3^-) transporters (9). Currently 10 members of the SLC26 family have been identified, and all members other than prestin have been shown to function as anion exchangers, with varying substrate specificities for a wide range of both monovalent and divalent anions, including chloride (Cl^-), bicarbonate (HCO_3^-), sulfate (SO_4^{2-}), iodide (I^-), hydroxyl ion (OH^-), oxalate, and formate (reviewed in 10). For example, while SLC26A2 transports both SO_4^{2-} and Cl^- (11), SLC26A4 (pendrin) mediates both Cl^-/I^- and Cl^-/formate exchange but is apparently not capable of transporting SO_4^{2-} (12,13). SLC26A6, which has ~56% homology to prestin, is capable of transporting all the above anions (14,15,16) and has been shown to operate as an electrogenic exchanger, exchanging more than one HCO_3^- ion for each Cl^- ion (16,17). However, although prestin possesses all the sequence domains conserved throughout the family, including a sulfate-transport motif (18), it has not yet been shown to function as an anion transporter. Moreover, neither gating charge movements nor a NLC have been reported for any other member of the SLC26 family, suggesting prestin may have a unique function within the family.

Although prestin has not been shown to transport Cl^-, the NLC associated with prestin was found to depend upon intracellular chloride, Cl_i (19,20). Thus, as for other members of the SLC26 family, prestin is likely to have at least one Cl_i binding site. Furthermore, the species of anion used to replace Cl^- in experimental conditions affects the dependence of the NLC on Cl_i (21,22), suggesting that, like other members of the SLC26 family, prestin can bind a broad range of substrates. At present, there is no consensus about the origin of the NLC and the nature of its dependence on Cl_i. This is partly a consequence of the contradictory experimental observations—that the NLC is abolished (19) or is

Submitted August 26, 2005, and accepted for publication February 27, 2006.

Address reprint requests to Jonathan Ashmore, Dept. of Physiology, UCL, Gower St., London WC1E 6BT UK. Tel.: 44-207-679-6080; E-mail: j.ashmore@ucl.ac.uk.

0006-3495/06/06/4035/11 $2.00

doi: 10.1529/biophysj.105.073254

not abolished (21) by complete removal of Cl_i. However, four key observations made in previous reports are clear:

I. β of the NLC is $\sim$0.03 mV^{-1}.
II. The peak NLC (C_{pk}) decreases as [Cl_i] is reduced.
III. The voltage at C_{pk} (V_o) shifts to more positive membrane potentials as [Cl_i] is reduced.
IV. The NLC is unaffected by removal of extracellular chloride (Cl_e) when [Cl_i] = 150 mM.

To achieve a better understanding of how prestin works, we have developed three kinetic types of model aiming to reproduce the key observations (I–IV). We find that a model of prestin as an anion exchanger provides a good description of the experimental observations.

Theory

All the models presented are described using simple kinetic diagrams, consisting of the intermediate states of the transporter protein (E_i) and transitions connecting these states. Each transition is described by a dielectric coefficient, which reflects the dielectric distance over which charge is translocated during the transition (23). Briefly, for a reaction step $E_i \rightarrow E_{i+1}$, in which an electric charge q_i is translocated across a fraction of the membrane dielectric δ_i, the dielectric coefficient for the transition, α_i is given as $\alpha_i = q_i\delta_i/e_o = \gamma_i\delta_i$, where γ_i is the magnitude of elementary charge translocated. All voltage-dependent reaction steps are treated as transitions over a symmetric energy barrier.

MATERIALS AND METHODS

Simulating NLCs

After a voltage perturbation, transitions through voltage-dependent reaction steps result in a measurable transient current $I(t)$, from which the measurable charge moved across the membrane, Q, and the NLC can be calculated. For a voltage-dependent reaction step, $E_i \leftrightarrow E_{i+1}$, Q is given by

$$Q = Ne_o\alpha_i \int k_f P_i(t) - k_b P_{i+1}(t)dt, \quad (2)$$

where N is the total number of transporters, e_o is the elementary charge, α_i is the dielectric coefficient for the reaction step, k_f is the forward transition rate, k_b is the backward transition rate, and $P_i(t)$ and $P_{i+1}(t)$ are occupancy probabilities of the states E_i, and E_{i+1}, respectively. If there is more than one voltage-dependent step then the total charge moved is the sum of that produced by each step.

The occupancy probabilities of the states from which voltage-dependent transitions occur were found using the spectral expansion of the Q-matrix, a method developed to describe transitions between ion channel states (24). Q was calculated for each step in a staircase voltage-ramp consisting of 1 mV steps between −200 mV and +200 mV. NLCs were calculated for a cell containing 10^7 copies of prestin. All simulations were performed in MatLab 6.5 (The MathWorks, Natick, MA).

For a given set of rate constants, NLCs were fitted to published data for [Cl_i] = 150 mM, 10 mM, 3 mM, and 1 mM and for [Cl_e] = 0 mM (19,20). Rate constants, comparable to those known for equivalent reaction steps in other transporters, were selected subject to two constraints:

1. In the dominant charge moving step, voltage-dependent rate constants were chosen to be at least 7×10^4 s^{-1}, since OHC electromotility can occur up to 70 kHz (25).
2. Unbinding rates were assumed to be fast and chosen to be 10^5 s^{-1}, similar to dissociation rates for fast binding and release from the aqueous phase.

Rate constants were varied to produce a NLC with V_o between –40 mV and –50 mV when [Cl_i] = 150 mM. Rate constants were optimized to minimize SSQ, the squared deviations between the data and the model, given by

$$SSQ = (RelC_{pkM} - RelC_{pkD})^2 + \frac{1}{\kappa^2}(\Delta V_{oM} - \Delta V_{oD})^2, \quad (3)$$

where $RelC_{pkM}$ and $RelC_{pkD}$ are relative C_{pk} for the model and data, respectively, and ΔV_{oM} and ΔV_{oD} are the shift in V_o for the model and data, respectively. The value κ is the maximum shift found for reduction of [Cl_i] to 1mM (20). Each rate constant was sequentially varied over the ranges described in Tables 1 and 2. Microscopic reversibility was maintained by simultaneously adjusting another otherwise unconstrained rate constant. It was found that the predictions for the shift in V_o depended critically on the binding rates of intracellular anions, while V_o for the NLC with [Cl_i] = 150 mM depended critically on the rate constants of the fast voltage-dependent step. Therefore, these rate constants were optimized first, and other rate constants were adjusted progressively to reduce SSQ.

Cell preparation and solutions

Young adult male albino guinea pigs (200–400 g) were killed by rapid cervical dislocation and both bullae were removed. Animal experiments were performed in accordance with local guidelines. The organ of Corti was dissected in HEPES-buffered solution containing (in mM): 145 NaCl, 5 KCl, 10 HEPES, 1 EGTA. Isolated OHCs were obtained by mechanical trituration after 15-min incubation in 0.25–0.5 mg/ml trypsin (T4665 from Bovine Pancreas, Sigma). The normal bath solution and the high Cl^- internal solution were identical and contained (in mM): 145 NaCl, 5 KCl, 10 HEPES, 1 EGTA. Cl^- concentrations were adjusted by replacing Cl^- with the divalent SO_4^{2-} and sucrose to give the equivalent ionic strength and osmolarity. Accordingly, 70 mM, 74.5 mM, and 75 mM SO_4^{2-} solutions were used for reduction of Cl^- to 10 mM, 1 mM, and 0 mM, respectively. All solutions were adjusted to pH 7.2–7.25 with NaOH and final osmolarity was adjusted to 310–315 mOsm with D-glucose. When Cl^--free bath solution was used, a 5% agar salt bridge containing 150 mM NaCl was used. Data were corrected for liquid junction potentials, which were calculated offline using a windows version of JPCalc (26) in Clampex 7.0 (Axon Instruments, Foster City, CA).

TABLE 1 Range of rate constants tested in simulations for the Cl^--transporter model

Rate constant	Range of values tested	Optimized rate constants
$k1$	10^6–10^8 M^{-1} s^{-1}	10^8 M^{-1} s^{-1}
k_{-1}	10^5 s^{-1}	10^5 s^{-1}
$k_2(0)$	7×10^4–42×10^4 s^{-1}	7×10^4 s^{-1}
$k_{-2}(0)$	7×10^4–42×10^4 s^{-1}	28×10^4 s^{-1}
$k_3(0)$	10–10^5 s^{-1}	10^4 s^{-1}
$k_{-3}(0)$	10–10^5 s^{-1}	10^5 s^{-1}
k_4	10^5 s^{-1}	10^5 s^{-1}
k_{-4}	10^6–10^7 M^{-1} s^{-1}	2.5×10^6 M^{-1} s^{-1}
k_5	0–10^5 s^{-1}	10^5 s^{-1}
k_{-5}	0–10^5 s^{-1}	10^5 s^{-1}

Optimization is achieved when $\alpha_1 = -0.8$, $\alpha_2 = -0.2$, so net charge movement occurs in the two transitions E1.Cl $\leftrightarrow$ E2.Cl, and E2.Cl $\leftrightarrow$ E3.Cl, and k_2, k_{-2}, k_3, and k_{-3} are voltage-dependent.

TABLE 2 Range of rate constants tested in simulations for the Cl^-/SO_4^{2-} exchanger model

Rate constant	Range of values tested	Optimized rate constants
k_1	10^6–10^8 M^{-1} s^{-1}	2.5×10^7 M^{-1} s^{-1}
k_{-1}	10^5 s^{-1}	10^5 s^{-1}
$k_2(0)$	7×10^4–35×10^4 s^{-1}	28×10^4 s^{-1}
$k_{-2}(0)$	7×10^4–35×10^4 s^{-1}	7×10^4 s^{-1}
$k_3(0)$	10–10^3 s^{-1}	2 s^{-1}
$k_{-3}(0)$	10–10^3 s^{-1}	100 s^{-1}
k_4	10^5 s^{-1}	10^5 s^{-1}
k_{-4}	10^3–10^8 M^{-1} s^{-1}	5×10^6 M^{-1} s^{-1}
k_5	10^3–10^8 M^{-1} s^{-1}	2.5×10^7 M^{-1} s^{-1}
k_{-5}	10^5 s^{-1}	10^5 s^{-1}
k_6	10–10^3 s^{-1}	200 s^{-1}
k_{-6}	10–10^3 s^{-1}	200 s^{-1}
k_7	10–10^3 s^{-1}	100 s^{-1}
k_{-7}	10–10^3 s^{-1}	10^3 s^{-1}
k_8	10^5 s^{-1}	10^5 s^{-1}
k_{-8}	10^6–10^8 M^{-1} s^{-1}	10^6 M^{-1} s^{-1}

Optimization is achieved when $\alpha_1 = 0.8$, $\alpha_2 = 0.2$, so net charge movement occurs in the two transitions E1.Cl↔E2.Cl and E2.Cl↔E3.Cl and k_2, k_{-2}, k_3, and k_{-3} are voltage-dependent.

Membrane capacitance recordings

Whole-cell voltage clamp recordings were carried out with 3.5–4.5 MΩ resistance electrodes using an Axopatch 200 A patch amplifier (Axon Instruments). All experiments were performed at room temperature (21–23°C). Voltage-dependent capacitance measurements were made using a conventional two-phase lock-in amplifier (SR350, Stanford Research, Menlo Park, CA). Command voltage was ramped from −130 mV to 100 mV over 8 s (29 mV s^{-1}) to ensure a close approximation to the steady state. The maximum error on NLCs measured with this protocol, which occurs in the type 3 model, was calculated and found to be <2%. Voltage ramps were summed with a 2 kHz, 10 mV sinusoid command. The first ramp was applied 10 s after break-in, to allow time to compensate the capacitive transients and were repeated every 18 s. The output of the lock-in amplifier was sampled at 256 Hz. Series resistance was not compensated, but the effect of series resistance on voltage was corrected offline.

Analysis of NLCs

Data was analyzed using MatLab 6.5. NLC traces were fitted with the derivative of a Boltzmann function, Eq. 1. Because dialysis of cells in whole-cell configuration proceeds exponentially (27), we fitted the time courses of V_o and C_{pk} with an exponentially decaying curve and obtained extrapolated values of V_o and C_{pk} at the instant of break-in ($t = 0$). The time courses of the shift in V_o from the instant of break-in ($\Delta V_o = V_o - V_o(0)$), and the relative decrease in C_{pk} from the instant of break-in ($relC_{pk} = C_{pk}/C_{pk}(0)$) were determined. Paired *t*-tests were used to test for significant changes in any parameter over time, by comparing the first and last time-point for each cell. In all other cases, two-tailed unpaired student *t*-tests were used to test for significance. All data are presented as mean ± SD.

RESULTS

Type 1 models: nontransporting modes of prestin

It has previously been proposed that prestin works as an incomplete transporter using intracellular chloride (Cl_i) ions as a voltage sensor without releasing Cl^- on the extracellular side (19). In this model, the Cl^- ion binds first at the mouth of the pore and is then translocated across the membrane to a second site at the top of the pore (Fig. 1 *A*). This three-state model can be described with a reaction scheme (Fig. 1 *B*), where E0, E1.Cl, and E2.Cl are also assigned to represent the number of prestin molecules in that state, respectively. The total number of prestin molecules (E_{tot}) is conserved, so

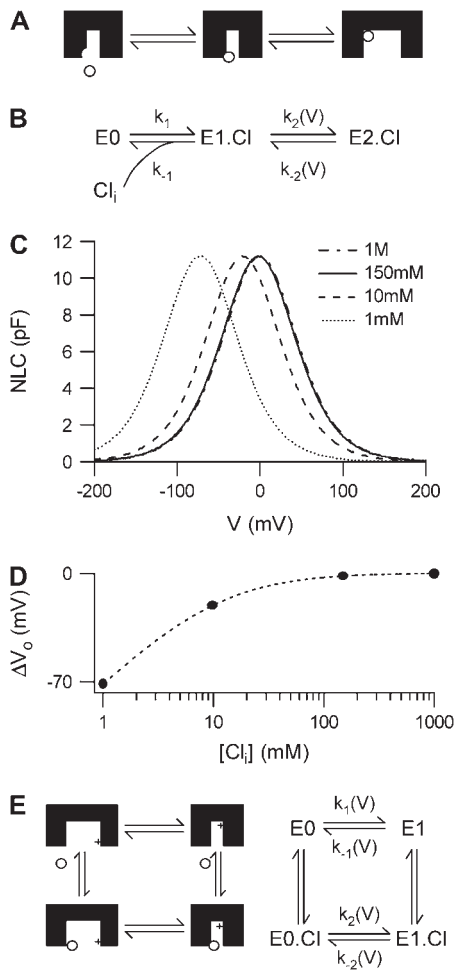

FIGURE 1 Nontransporting models of prestin. (*A*) An incomplete transport model of prestin. Prestin changes from a contracted to an expanded state when a Cl^- ion moves from the first binding site at the mouth of the pore to a second site at the top of the pore. All charge movement is provided by the translocation of the Cl^- ion. (*B*) The reaction scheme used to describe this model. (*C*) The NLC produced by the model depends on $[Cl_i]$. In the example shown $K_D(Cl_i) = 10$ mM, $k_2(0) = k_{-2}(0) = 10^4$ s^{-1}. There is a negative shift in V_o but no change in C_{pk} as $[Cl_i]$ is reduced. Note that the traces for 150 mM and 1 M are superimposed. (*D*) The shift in V_o (ΔV_o) for the example shown in panel *C*. ΔV_o is always negative when $[Cl_i]$ is reduced and approaches zero as $[Cl_i]$ increases. The dotted line represents Eq. 10 with ΔV_o calculated relative to the V_o for 1 M $[Cl_i]_1$. (*E*) An alternative model of prestin, where prestin changes from an expanded to a contracted state when an intrinsic positively charged sensor is moved across the membrane. All charge movement is provided by the translocation of the intrinsic charged sensor. Cl_i binds to a distinct site, altering the rate of charge movement ($k_{-2}(V)/k_2(V) \neq k_{-1}(V)/k_1(V)$). In this and subsequent figures, inside facing surfaces of the schematic molecule is down.

$$E_{tot} = E0 + E1.Cl + E2.Cl. \quad (4)$$

The binding and unbinding of Cl^- is assumed to be voltage-independent. The dissociation constant for the Cl^--binding step is given by

$$K_D(Cl_i) = \frac{k_{-1}}{k_1}. \quad (5)$$

The transition between the bound states of prestin (E1.Cl↔E2.Cl) is associated with charge translocation so the step depends on membrane potential (V). The forward and backward rate constants for the transition between the bound states are given by

$$k_2(V) = k_2(0)e^{\frac{\alpha e_o V}{2k_B T}}, \quad (6)$$

$$k_{-2}(V) = k_{-2}(0)e^{-\frac{\alpha e_o V}{2k_B T}}, \quad (7)$$

where α is the dielectric coefficient. Since all charge movement is provided by the movement of the Cl^- ion, $\alpha = z\delta$ where z ($= -1$) is the valence of the Cl^- ion, and δ is the fraction of the membrane dielectric crossed by the Cl^- ion.

In this model, hyperpolarization forces Cl^- toward the extracellular surface since α is negative. As OHCs elongate upon hyperpolarization, we associate this transition with a conformational change of prestin into an expanded state (8). Since charge is transferred across the membrane every time a prestin molecule makes the transition from the state E1.Cl to the state E2.Cl, the total charge transferred, Q is proportional to the number of prestin molecules in the state E2.Cl. The number of prestin molecules in the state E2.Cl at equilibrium, is found using Eqs. 4–7:

$$E2.Cl = \frac{E_{tot}}{1 + \frac{k_{-2}(V)}{k_2(V)}\left(1 + \frac{k_{-1}}{k_1[Cl_i]}\right)}. \quad (8)$$

Q therefore depends on both V and $[Cl_i]$. When Cl_i is completely removed no charge transfer occurs, and consequently the associated NLC is abolished. As Q is proportional to E2.Cl, the maximum charge transferred, Q_{max} corresponds to the condition that all the prestin molecules are in the state E2.Cl. Assuming that more Cl^- ions than prestin molecules are present, all the prestin molecules can be forced into the state E2.Cl, by increasing the hyperpolarizing driving force ($k_2(V)$) sufficiently, regardless of $[Cl_i]$. Therefore contrary to experimental observations Q_{max}, which is proportional to C_{pk} ($C_{pk} = \beta Q_{max}/4$, from Eq. 1) is constant for all $[Cl_i] > 0$ and only depends on the total number of prestin molecules present.

The V_o of the NLC occurs when half the maximal charge has been transferred. Using Eq. 8, V_o can be calculated as

$$V_o = \frac{k_B T}{\alpha e_o}\ln\left(\frac{k_{-2}(0)}{k_2(0)}\left(1 + \frac{k_{-1}}{k_1[Cl_i]}\right)\right). \quad (9)$$

Clearly, V_o depends on $[Cl_i]$ and becomes more negative as $[Cl_i]$ is reduced (Fig. 1 *C*). The shift in V_o due to a change in $[Cl_i]$ from a first concentration, $[Cl_i]_1$ to a second concentration, $[Cl_i]_2$ is found directly from Eq. 9 as

$$\Delta V_o = \frac{k_B T}{\alpha e_o}\ln\left(\frac{1 + \frac{k_{-1}}{k_1[Cl_i]_2}}{1 + \frac{k_{-1}}{k_1[Cl_i]_1}}\right). \quad (10)$$

Thus this model predicts a negative shift in V_o whenever $[Cl_i]_2 < [Cl_i]_1$. This is in the opposite direction to that observed experimentally when $[Cl_i]$ is reduced (Fig. 1 *D*).

An alternative nontransporting model of prestin has also been proposed (21), in which it is suggested that the NLC is generated by an intrinsic voltage-sensor, and the dependence of the NLC on $[Cl_i]$ is due to an allosteric action of Cl^- binding to a site, distinct from the voltage-sensing residues. Such a model is illustrated in Fig. 1 *E*. In this model Q_{max} and consequently C_{pk} corresponds to the case that all the prestin molecules are in the state E1 or E1.Cl. As with the first model, this condition can be achieved by increasing the driving force ($k_1(V)$ and/or $k_2(V)$) sufficiently, regardless of $[Cl_i]$. Therefore, although this model might account for the observed shifts in V_o, it likewise cannot account for the decrease in C_{pk} observed.

Type 2 models: chloride-transporting mode

It is clear that the previous class of nontransporting models cannot reproduce the key experimental observations (I–IV, above). Since prestin belongs to a family of anion exchangers, we have developed a model in which prestin completes a full transport cycle, transporting Cl^- across the membrane (Fig. 2 *A*). In this model a Cl^- ion binds to a binding site facing the intracellular medium, then moves through the membrane to a second site accompanied by a conformational change from where Cl^- moves to a third site facing the extracellular medium and is released. Finally prestin returns to the inward facing state with no ion bound.

The reaction scheme for this model is shown in Fig. 2 *B*. We assume that the Cl^- ion crosses the whole membrane dielectric within the two transitions, E1.Cl↔E2.Cl and E2.Cl↔E3.Cl. The binding and unbinding of both Cl_i and Cl_e are assumed to be voltage-independent. If the dielectric coefficients for the transitions E1.Cl↔E2.Cl and E2.Cl↔E3.Cl are α_1 and α_2, respectively, then the rate constants for the two transitions are

$$k_2(V) = k_2(0)e^{\frac{\alpha_1 e_o V}{2k_B T}}, \quad (11)$$

$$k_{-2}(V) = k_{-2}(0)e^{-\frac{\alpha_1 e_o V}{2k_B T}}, \quad (12)$$

$$k_3(V) = k_3(0)e^{\frac{\alpha_2 e_o V}{2k_B T}}, \quad (13)$$

$$k_{-3}(V) = k_{-3}(0)e^{-\frac{\alpha_2 e_o V}{2k_B T}}. \quad (14)$$

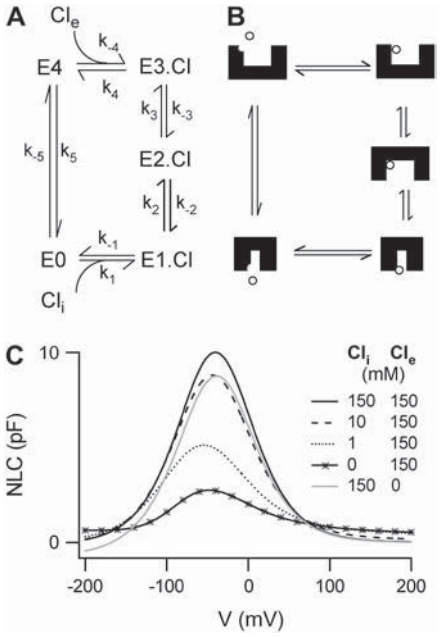

FIGURE 2 A chloride transporting model. (*A*) The reaction scheme used to describe a chloride transporting model. Cl^- binds to a binding site facing the intracellular medium. It is then transported across the membrane where it is released to the extracellular medium, before prestin returns to the unbound inward facing state. All charge movement is provided by the translocation of the Cl^- ion. (*B*) Since hyperpolarization increases the forward rate of the transition E1.Cl↔E2.Cl, we associate this transition with a conformational change of prestin into an expanded state (8). Furthermore, since the occupancy of the outward facing state E4 is increased by removal of Cl_i, and OHCs elongate in low Cl_e (33), the state E4 is provisionally assigned an expanded conformation. All other states are assigned conformations to fit with these constraints. (*C*) This transporter model reproduces aspects of previous experimental observations. C_{pk} decreases as $[Cl_i]$ is reduced and there is little effect of removing Cl_e in the presence of high $[Cl_i]$. However, unlike experimental observations, a negative shift in V_o is produced as $[Cl_i]$ is reduced.

Since all charge movement is provided by the translocation of the Cl^- ion, $\alpha_1 = z\delta_1$, $\alpha_2 = z\delta_2$ with $\delta_1 + \delta_2 = 1$, where $(z = -1)$ is the valence of the Cl^- ion and δ_1 and δ_2 are the fraction of the membrane dielectric crossed by the Cl^- ion in the transitions.

In model simulations, two particular cases were considered. In the first case, the Cl^- ion crosses 100% of the membrane dielectric in the first transition resulting in one voltage-dependent step ($\alpha_1 = -1$, $\alpha_2 = 0$) and NLCs with $\beta \sim 0.04\ mV^{-1}$, in poor agreement with the data. In the second case, the Cl^- ion crosses 80% of the membrane dielectric in the first transition and 20% of the membrane dielectric in the second transition, resulting in two voltage-dependent steps ($\alpha_1 = -0.8$, $\alpha_2 = -0.2$), and NLCs with $\beta \sim 0.03\ mV^{-1}$ in agreement with the experimental observations. Since the mechanism obeys microscopic reversibility, there are nine independent rate constants for this model. Table 1 shows the range of rate constants tested. With rate constants optimized, the NLC for $[Cl_i] = 150$ mM gives $V_o = -40$ mV, and $\beta = 0.032\ mV^{-1}$. For all combinations tested, the model produces a decrease in C_{pk} when $[Cl_i]$ is reduced if transitions between the inward and outward facing states can occur without Cl^- bound. No combination of rate constants tested produces a positive shift in V_o.

The origin of the decrease in C_{pk} can be understood in the following way: when voltage is changed from very negative to very positive potentials, transitions are caused from the state E3.Cl toward the state E1.Cl. This produces the observed charge movement. The maximum possible charge movement occurs if all prestin molecules undergo transitions from the state E3.Cl to the state E1.Cl. When $[Cl_i]$ is reduced, the equilibrium shifts toward E4 and E3.Cl so the population of E3.Cl is maintained even at very positive potentials. This permits fewer transitions associated with a charge movement. Hence, C_{pk} is reduced. Since in this model Cl^- is moved across the membrane by hyperpolarization, a reduction in $[Cl_i]$ shifts the equilibrium further away from the states E2.Cl and E3.Cl and toward the state E1.Cl. Thus a greater hyperpolarizing driving force is required to produce as much charge transfer, resulting in a negative shift in V_o as $[Cl_i]$ is reduced. In principle, it is possible to produce a positive shift in V_o with this model, provided that transitions E0↔E4 and E2.Cl↔E3.Cl are considerably faster than the critical voltage-dependent step, E1.Cl↔E2.Cl. In such a case, the equilibrium shifts further toward the state E2.Cl as $[Cl_i]$ is decreased. However, the required rate constants for the transitions E0↔E4 and E2.C↔E3.Cl would lie beyond the range we have considered reasonable for a transporter protein.

As expected for a cyclic model, the NLC curve does not asymptote to zero, when $[Cl_i]$ is low or Cl_e is removed. This is because the transition E0↔E4 prevents the occupancy of any state from fully saturating and permits an incremental charge movement for any further membrane potential change. Furthermore, in zero Cl_e, the transition E0↔E4 causes the equilibrium to shift toward the state E2.Cl at very negative V_m, and leads to charge moving in the opposite direction. This produces a small negative NLC. The asymptotic dependence on $[Cl_i]$ was not analyzed in further detail because these effects are only observable outside the range of potentials (−100 mV to 100 mV) usually measured.

Type 3 models: anion antiporter mode, with intrinsic charge movement

The Cl^- transporting model shows that in a cyclic model where Cl^- is fully transported across the membrane, a decrease in C_{pk} is a consequence of reduced $[Cl_i]$. However, none of the previous models, in which the only charge movement is provided by the translocation of a Cl^- ion, can produce a positive shift in V_o as $[Cl_i]$ is reduced. Therefore, we adapted the transporter model to include the movement of intrinsic charged residues. Such movement might occur during a conformational change in the protein.

Consider a Cl^- transporter model, with the same reaction scheme as that shown in Fig. 2 *B*, but with the movement of Cl^- accompanied by the movement of intrinsic positively charged residues, so that there is a net movement of positive charge when Cl^- is transported from the intracellular surface of the membrane toward the extracellular surface. During a complete cycle, the intrinsic charged residues must be returned to their original position, requiring an additional voltage-dependent step. When this is incorporated, the output of the model compares poorly with experimental observations (data not shown).

Since other members of the SLC26 family typically operate as antiporters, and since previous experimental observations have indicated that prestin interacts with a broad range of anions, we considered a model of prestin as an anion exchanger. The key property of this model is that prestin mediates electrogenic exchange, exchanging 1 Cl^- ion for a divalent anion, X^{2-}. In this model, the reorientation of the intrinsic positively charged residues only occurs with X^{2-} bound. This effectively neutralizes the positive charge such that no net charge is moved when X^{2-} is transported across the membrane. Thus, both the translocation of X^{2-} and the reorientation of the intrinsic charged residues are electroneutral and there is no longer any requirement for additional voltage-dependent steps.

Since SO_4^{2-} has previously been used to substitute for Cl^- in experiments, we implemented this model explicitly as a Cl^-/SO_4^{2-} exchanger, exchanging one Cl^- ion for one SO_4^{2-} ion (Fig. 3 *A*). Two possible conformational state assignments are shown in Fig. 3, *B* and *C*. Both assignments produce the correct electromotile length-voltage relationship (Fig. 3 *E*). As with the Cl^- transporter model it is assumed that the Cl^- ion crosses the whole membrane dielectric within the two steps E1.Cl↔E2.Cl and E2.Cl↔E3.Cl. All other transitions are assumed to be voltage-independent.

Charge movement is provided by the translocation of the Cl^- ion combined with the movement of intrinsic positively charged residues. If the dielectric coefficients for the transitions E1.Cl↔E2.Cl and E2.Cl↔E3.Cl are α_1 and α_2, respectively, then the rate constants for the two transitions are the same as those given in Eqs. 9–12. But since charge movement is provided by the translocation of the Cl^- ion and intrinsic charged residues $\alpha_1 = z\delta_1 + \mu_1$ and $\alpha_2 = z\delta_2 + \mu_2$ with $\delta_1 + \delta_1 = 1$, where z ($= -1$) is the valence of the Cl^- ion, δ_1 and δ_2 are the fraction of the dielectric crossed by the Cl^- ion in the transitions, and μ_1 and μ_2 are the contributions due to the intrinsic charge movement.

In a single cycle the equivalent of a positively charged ion with a valence of +1 is transferred from inside to outside. Charge conservation requires that

$$\alpha_1 + \alpha_2 = 1, \text{ hence } \mu_1 + \mu_2 = 2. \quad (15)$$

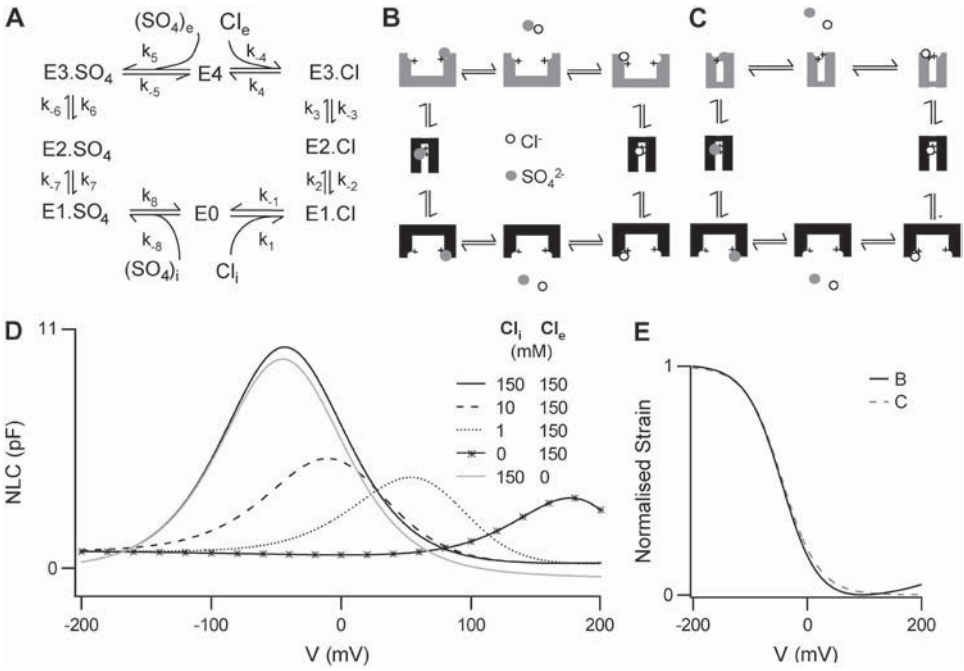

FIGURE 3 A chloride/sulfate antiporter model. (*A*) The reaction scheme for a Cl^-/SO_4^{2-} exchanger model. Prestin exchanges one Cl^- ion for one SO_4^{2-} ion via an alternating-access mechanism, in which prestin can only change between inward and outward facing states with an anion bound. Charge movement is provided by the translocation of a Cl^- ion and some intrinsic positively charged residues. Thus net positive charge is moved across the membrane as the Cl^- ion is moved toward the extracellular surface. The reorientation of the intrinsic positively charged residues occurs with a SO_4^{2-} ion bound, which neutralizes the positive charge, so the translocation of SO_4^{2-} is voltage-independent. (*B*,*C*) Two alternative representations of the reaction scheme. Both assignments ensure that the critical voltage-dependent transition, E1.Cl↔E2.Cl, is associated with a conformational change of prestin into a compact state and symmetry is maintained (8). (*D*) The exchanger model reproduces most aspects of previous experimental observations. There are large positive shifts in the V_o of the NLC and C_{pk} decreases as $[Cl_i]$ is reduced. There is little effect of removing Cl_e, in the presence of high $[Cl_i]$. For $[Cl^-] = 10$, 1 or 0 mM, $[SO_4^{2-}]$ was 70, 74.5, or 75 mM, respectively. (*E*) Normalized strain versus membrane potential. Within the range of potentials usually measured (−100 mV to 100 mV), both representations *B* and *C* predict a sigmoidal dependence of length on potential. Depolarization causes shortening associated with an accumulation of compacted states, and hyperpolarization causes lengthening associated with an accumulation of expanded states.

In simulations, two particular cases were considered. In the first case, the Cl^- ion and the equivalent of two positively charged residues crosses 100% of the membrane dielectric in the first transition ($\alpha_1 = 1$, $\alpha_2 = 0$), resulting in NLCs with $\beta \sim 0.04$ mV^{-1}. In the second case, the Cl^- ion and the equivalent of two positively charged residues crosses 80% of the membrane dielectric in the first transition and 20% of the membrane dielectric in the second transition ($\alpha_1 = 0.8$, $\alpha_2 = 0.2$), resulting in NLCs with $\beta \sim 0.03$ mV^{-1}. Because this mechanism obeys microscopic reversibility, there are 15 independent rate constants for this model. Table 2 shows the range of rate constants tested.

The Cl^-/SO_4^{2-} exchanger model produces a decrease in C_{pk} on reducing $[Cl_i]$ for all combinations of rate constants. Furthermore, since in this model the Cl^- is moved across the membrane by depolarization, a positive shift in V_o is also produced. With rate constants optimized, the K_D for Cl_i is 4 mM and the K_D for $(SO_4)_i$ is 100 mM. The NLC produced for $[Cl_i] = 150$ mM gives $V_o = -43$ mV and $\beta = 0.032$ mV^{-1}, in agreement with the experimental observations. When $[Cl_i]$ is reduced to 10 mM or to 1 mM there is both a large positive shift in V_o (by 30.5 mV or 97.9 mV) and a decrease in C_{pk} (to 42% of max, or 34% of max, respectively) (Fig. 3 *C*). When Cl_i is completely removed a significant NLC remains (18% of max), but its V_o is shifted to very positive membrane potential ($V_o = 175$ mV). There is little effect on the NLC of removing Cl_e when $[Cl_i] = 150$ mM.

By its nature, this model has the latitude to account for the dependence of the NLC on the replacement anion where the replacement anion is divalent. However, the observations (I–IV) were also found in experiments where monovalent anions were used to replace Cl^- (21,22). Therefore we tested the behavior of the model with two monovalent anions (A^-) substituting for SO_4^{2-}. The two monovalent anions bind in two sequential steps, are transported across the membrane together, and then dissociate in two sequential steps. Since the two anions are transported across the membrane together, this is the charge equivalent of translocating one SO_4^{2-} anion across the membrane, so the translocation of $2A^-$ is electroneutral and produces no charge movement. Like the Cl^-/SO_4^{2-} exchanger, the $Cl^-/2A^-$ exchanger model also produces a decrease in C_{pk} and positive shift in V_o as $[Cl_i]$ is reduced.

Replacing chloride with sulfate in whole-cell recordings

Although previous experimental reports have consistently shown that replacing Cl_i with SO_4^{2-} produces large positive shifts in V_o, there were discrepancies regarding the effects on C_{pk} (20,21). To compare the quantitative predictions of the Cl^-/SO_4^{2-} exchanger model with experimental data, additional experiments to test the effect on the NLC of replacing Cl_i with SO_4^{2-} were performed.

When cells were patched with 150 mM Cl^- in the pipette solution, no shift in V_o or decrease in C_{pk} was observed (Fig. 4 *A*), suggesting that the $[Cl_i]$ in the cell before break-in was sufficiently high that any further increase in $[Cl_i]$ up to 150 mM does not alter the NLC. When cells were patched with a low Cl^- concentration in the pipette solution there was a positive shift in V_o and a decrease in C_{pk}, as the ionic concentration in the cell reached the same concentration as in the pipette solution. Steady-state values were reached within 3–5 mins, consistent with previous reports (21,22). Since $[Cl_i]$ in the cell before break-in produced the same NLC as 150 mM $[Cl_i]$, these changes were assumed to be identical to those that would be observed for a reduction of $[Cl_i]$ from 150 mM to the Cl^- concentration in the pipette solution.

Accordingly when $[Cl_i]$ was reduced to 10 mM or to 1 mM there was a positive shift in V_o (by 55.6 ± 15.2 mV or 84.6 ± 13.0 mV, respectively), a decrease in C_{pk} (to 49.0 ± 13.6% of max, or 45.8 ± 15.8% of max, respectively), and no change in β ($p > 0.1$). Although the shift in V_o was significantly greater when $[Cl_i]$ was reduced to 1 mM ($p < 0.05$), C_{pk} did not differ significantly ($p > 0.7$). The experimental measurements made here and those from previously published data (19,20) are compared with the predictions of the model in Fig. 4 *B*.

The model predicts that a considerable NLC will remain if Cl_i is removed. When cells were patched with Cl^--free solution we found a residual NLC (Fig. 5 *A*). The C_{pk} of the residual NLC was within two SDs of that predicted by the model (32.4 ± 9.5% of max compared with 25% of max), whereas the shift in V_o was considerably smaller than predicted by the model (by 81.7 ± 9.8 mV compared with a predicted 218 mV). These measured values did not differ significantly from those when cells were patched with 1 mM Cl^- in the pipette solution ($p > 0.2$).

If Cl^- is removed from both internal and external solutions, the model predicts that the NLC should be abolished, since transport of SO_4^{2-} is voltage-independent. To ensure all Cl^- was completely washed out, cells were bathed and dissected in Cl^--free solution and patched with Cl^--free solution to ensure no exogenous source of Cl^- was presented to the cells. Ten seconds after break-in a considerable NLC was detected in all cells (Fig. 5 *B*). However, the mean C_{pk} of the NLC (3.07 ± 1.31 pF, $n = 13$) was significantly smaller ($p < 0.01$) than that observed when cells were bathed in a high Cl^- bath solution (7.2 ± 3.5 pF, $n = 19$). In addition, the mean V_o of the NLC (38.4 ± 16.8 mV, $n = 13$) was significantly more positive ($p < 0.01$) than that observed when cells were bathed in a high Cl^- bath solution (−40.3 ± 10.9 mV, $n = 19$). This implies that the $[Cl_i]$ in the cells before break-in was depleted by bathing in Cl^--free solution. After break-in, the C_{pk} of the NLC decreased and the V_o of the NLC appeared to shift to more positive potentials, such that in later recordings the peak of the NLC was not observable within the range of potentials recorded. Unfortunately it proved not possible to extend the

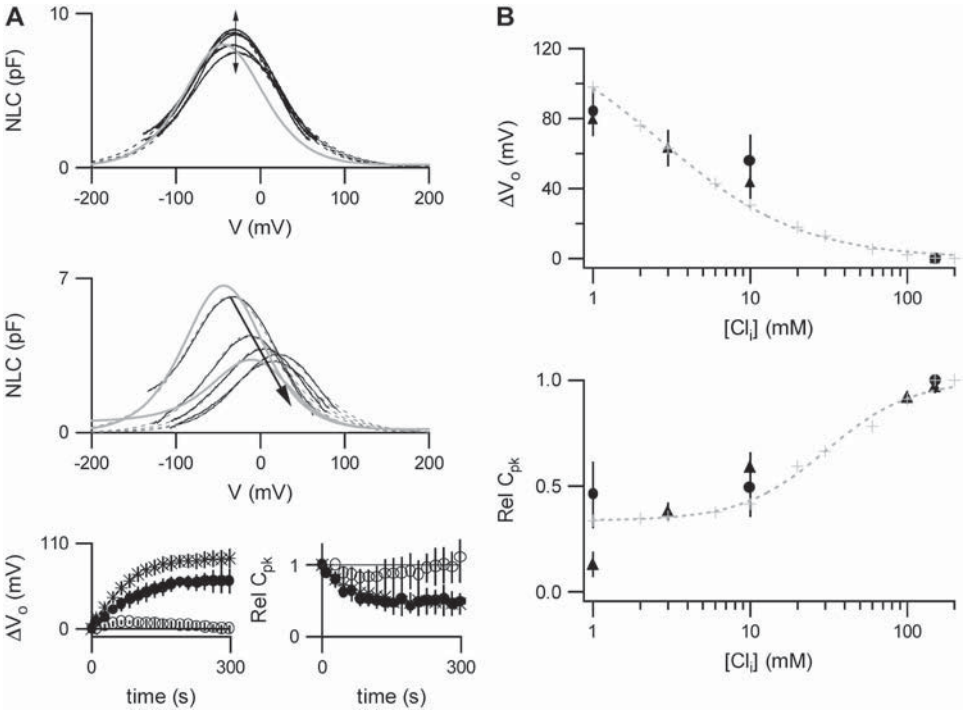

FIGURE 4 The dependence of the NLC on $[Cl_i]$ when Cl_i is replaced with SO_4^{2-}. (*A*) NLCs were recorded in the whole-cell configuration with a $[Cl_i]$ of 150 mM ($n = 7$), 10 mM ($n = 5$), or 1 mM ($n = 4$). Traces are shown at 54-second intervals, from the first record. The dotted lines show the fits of the derivative of the Boltzmann function (Eq. 1) to the NLC traces. The model predictions are shown in gray. The top panel shows an example of a cell patched with 150 mM $[Cl_i]$. No change in NLC over time was observed. The prediction of the model is scaled to the C_{pk} measured at break-in ($t = 10$ s). The middle panel shows an example of a cell patched with 10 mM $[Cl_i]$. After break-in there was a positive shift in the V_o of the NLC and C_{pk} decreased. The model predictions were scaled to the maximum C_{pk}, which was estimated for the instant of break-in ($t = 0$). The bottom panel shows the mean time courses of the shift in $V_o(\Delta V_o)$ and the relative change in C_{pk} ($RelC_{pk}$) after break-in, for cells patched with 150 mM (○), 10 mM (●), and 1 mM (*) Cl^-. There was no shift in V_o or any change in C_{pk} for cells patched with 150 mM $[Cl_i]$. There was a positive shift in V_o and a decrease in C_{pk} when cells were patched with 10 mM or 1 mM. Note $RelC_{pk}$ for 10 mM and 1 mM are superimposed. (*B*) A comparison of experimental measurements of the dependence of NLC on $[Cl_i]$ with the predictions of the Cl^-/SO_4^{2-} exchanger. The predictions of the model are shown in gray. Fitting a logistic Hill function to the shift in V_o gives a $K_{1/2}$ and Hill coefficient for Cl_i of 2.7 ± 0.4 mM and 0.97, respectively. Fitting $RelC_{pk}$ gives a $K_{1/2}$ and Hill coefficient for Cl_i of 30 ± 3 mM and 1.6, respectively. The values for ΔV_o and $RelC_{pk}$ from those measurements in excised patches (▲) taken from (19,20) and those obtained here from whole-cell recordings (●) are shown for comparison with the predictions of the model. All data is shown as mean ± SD.

range of potentials recorded without compromising the stability of the recording, and fitting of the derivative of the Boltzmann function (Eq. 1) to the visible parts of the traces was highly sensitive to the choice of initial parameters. Nevertheless, it appeared that a residual NLC remained, with its V_o shifted to potentials more positive than 100 mV. Thus, contrary to the predictions of the model, it appears that the NLC was not abolished by the removal of both Cl_i and Cl_e.

DISCUSSION

To date, two alternative nontransporting models of prestin have been proposed. Experimental observations that the NLC was abolished by removal of Cl_i, but was unaffected by removal of Cl_e, led to the proposal that prestin uses extrinsic Cl_i ions as a voltage-sensor (19). Later contrasting experimental observations showed that a residual NLC remained in the absence of Cl_i, which led to the proposal that the NLC was generated by an intrinsic voltage-sensor, and the dependence of the NLC on $[Cl_i]$ was due to an allosteric action of Cl^- on prestin (21,22). In this article we have shown that both these nontransport models of prestin, whether using Cl^- as a voltage-sensor or an intrinsic charged sensor, cannot account for the experimental observations, since no decrease in C_{pk} can be produced.

We suggest a third model in which prestin acts as an electrogenic anion exchanger, but one in which the charge movement arises as a result of both a Cl^- ion and intrinsic charged residues moving across the membrane. This model is independent of the nature of the Cl^- replacing anion, which could be mono- or divalent as long as it guarantees that the reorientation of the intrinsic charged residues is electroneutral. As an implementation of this concept we used previously published data, which described the Cl^- dependence of the NLC when SO_4^{2-} was used to replace Cl^- (19), to constrain our model and subsequently tested the predictions with additional measurements on dissociated OHCs. This Cl^-/SO_4^{2-} exchanger model provides the first semi-quantitative description of the experimental observations.

Is chloride required to generate an NLC?

A major issue in all possible models of prestin is whether Cl^- is required to generate the NLC. Although the Cl^-/SO_4^{2-} exchanger model presented here includes the movement of intrinsic charges, it also requires the presence of Cl^- to generate a NLC. Thus, in the absence of either Cl_i or Cl_e no NLC would be produced. Instead, we found a residual NLC, shifted to very positive potentials ($V_o > 100$ mV) when experiments were performed under these conditions. There

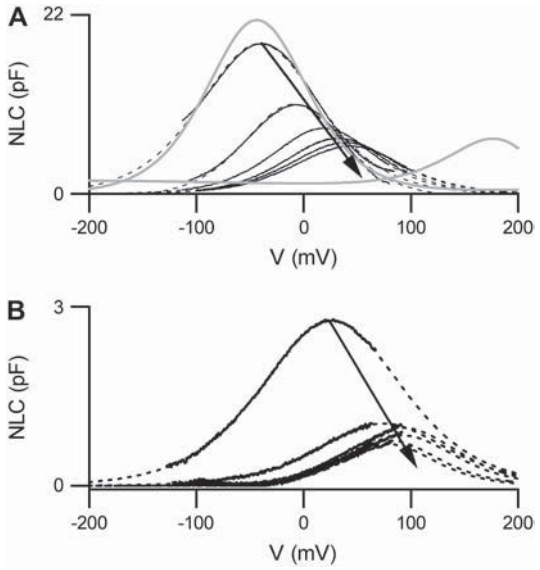

FIGURE 5 Residual NLCs remain in the absence of chloride. NLCs were recorded in the whole-cell configuration with either Cl_i completely replaced with SO_4^{2-} ($n = 3$), or with both Cl_i and Cl_e completely replaced with SO_4^{2-} ($n = 13$). Where both Cl_i and Cl_e were replaced, cells were dissected and bathed in Cl^--free solution to ensure complete removal of Cl^- from both internal and external solutions. Traces are shown at 54 s intervals, from the first record. The dotted lines show the fits of the derivative of the Boltzmann function (Eq. 1) to the NLC traces. Model predictions are shown in gray. (*A*) Example of a cell patched with Cl^--free solution, in a high-Cl^- bath solution. The model predictions were scaled to the maximum C_{pk}, which was estimated for the instant of break-in ($t = 0$). A considerable NLC remained when Cl_i was completely removed. The V_o of the NLC shifted to a more positive potential and C_{pk} decreased. The shift in the NLC was much smaller than that predicted by the model. (*B*) Example of a cell patched in Cl^--free solution in a Cl^--free bath. An NLC was present in all cells bathed in Cl^--free solution at break-in. After break-in the V_o of the NLC shifted to a more positive potential, such that it was beyond the range of V measured. Attempts to fit the visible part of the trace were uncertain.

are at least two possible explanations for this: 1), an alternative anion such as HCO_3^- may substitute for Cl^- to generate a NLC; or 2), Cl^- cannot be completely removed, due to Cl^- initially present in the OHC cytoplasm, or contamination of salts used to make up solutions. In fact, contrary to previous assumptions, the model predicts that even if $[Cl_i]$ and $[Cl_e]$ are only 10 μM, there is a considerable NLC, with a $C_{pk} = 56\%$ of max and $V_o = 216$ mV, which is compatible with experimental observations.

In contrast, removal of Cl_i only is not expected to abolish the NLC, since Cl^- is still available from the extracellular medium. However, the NLC predicted by the model was not detected in either whole-cell experiments described here, nor in previous experiments on excised patches (19). In the whole-cell experiments, although residual NLC was detected, neither the decrease in C_{pk} nor the shift in V_o were as large as those predicted, while in excised patch experiments the NLC appeared to be abolished (19). One explanation for the discrepancy observed between the predicted NLC and the NLC observed in whole-cell recordings is that it is not possible to completely remove Cl_i in the whole-cell configuration. This is supported by a recent study, which showed that the presence of a Cl^- conductance serves to counteract pipette washout when there is a large Cl^- gradient (22). On the other hand, in excised patches, where Cl_i can be effectively removed, but the signal is smaller due to fewer prestin molecules, the predicted NLC may not be detected since its V_o lies far beyond the range of potentials measured.

A chloride conductance associated with the model

The anion exchanger model of prestin proposes that prestin mediates electrogenic exchange and therefore it should be possible to identify its transport properties using electrophysiological techniques. The effect of removing either Cl_i or Cl_e on the $I(V)$ of an OHC can be predicted for a Cl^-/SO_4^{2-} exchanger. The consequences were calculated using the same optimized rate constants shown in Table 2. Complete removal of Cl_i shifts the reversal potential to an infinitely positive potential, and leads to an inward current of ~80 pA at a holding potential of 0 mV (Fig. 6). Complete removal of Cl_e shifts the reversal potential to an infinitely negative potential, and leads to a very small outward current of ~2.5 pA at a holding potential of 0 mV. The magnitudes of these currents are a consequence of the slow transitions $E2.Cl \leftrightarrow E3.Cl$, and $E2.SO_4 \leftrightarrow E3.SO_4$. When 150 mM Cl^- is present inside and outside the cell, no steady-state current will be observed at any potential since no full cycle can occur. However, if prestin were able to mediate $Cl^-/2Cl^-$ exchange in this condition, prestin would behave as a Cl^- uniporter, resulting in an $I(V)$ that reverses at 0 mV (not shown).

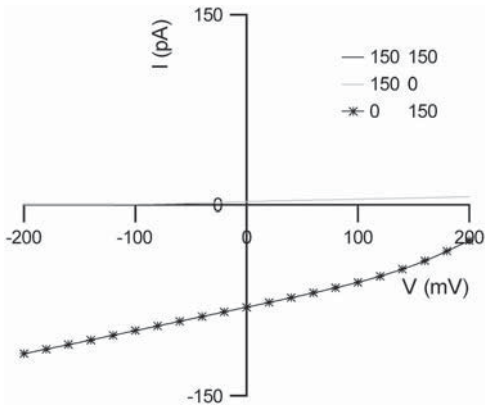

FIGURE 6 Predicted $I(V)$s for the chloride/sulfate exchanger model. No steady-state current is produced when $[Cl_i] = [Cl_e] = 150$ mM. Removal of Cl_i leads to a positive shift in the reversal potential and an increase in inward current at 0 mV. Removal of Cl_e leads to a negative shift in the reversal potential and an increase in outward current at 0 mV. 75 mM SO_4^{2-} was used to replace Cl^- completely.

Is prestin likely to function as an exchanger in vivo?

In vivo, receptor potentials in OHCs vary continuously and in response OHCs change their length, generating force that is fed back into the basilar membrane. We suggest that prestin is driving this process by means of an anion exchange cycle, in which one or more states are expanded, which can be driven by either transmembrane potential or anion gradients.

The results presented here indicate that prestin might be able to function as a Cl^-/SO_4^{2-} exchanger. Cl^- is a likely substrate in vivo, since it is believed to be present in the cell at millimolar concentrations in vivo, with estimates for the resting $[Cl_i]$ in isolated cells ranging from ~8–20 mM (22,28). However, there is no evidence that SO_4^{2-} is present in OHCs or the fluids surrounding OHCs. Considering that at least two of the anion exchangers in the SLC26 family (SLC26A3 and SLC26A6) mediate both Cl^-/SO_4^{2-} exchange and Cl^-/HCO_3^- exchange, it is possible that rather than mediating Cl^-/SO_4^{2-} exchange in vivo, prestin mediates Cl^-/HCO_3^- exchange. The presence of a Cl^-/HCO_3^- exchanger in OHCs has previously been suggested by evidence that in isolated OHCs, the intracellular pH depended on $[Cl_e]$ (29).

However, the unusually high density of prestin compared with other transporters suggests its primary function is to drive electromotility, and it is unlikely that it also plays the critical role in regulating Cl_i. In fact, several other Cl^- transporters and channels have already been implicated to perform Cl_i regulation. ClC channels have been identified in OHCs by RT-PCR (30,31) and the Cl^-/HCO_3^- exchanger SLC4A2 (AE2) has been identified in OHCs via a combination of RT-PCR and immunohistochemistry (32), although so far there is no evidence to show that any of these proteins are localized at the cell membrane or are functional. Since at present it remains unclear which channels, and transporters are responsible for regulating $[Cl_i]$ in OHCs, it is difficult to predict the extent to which prestin may contribute to the regulation of Cl_i and thereby help to set its own voltage-sensitivity. In practice, the turnover of prestin at physiological concentrations of substrates may be so low as to render its transport properties inconsequential. Instead, it may use its transport properties to create a motor that is sensitive to both voltage and anion gradients created by other channels.

APPENDIX

Derivation of Eq. 9

The reaction scheme described in Fig. 1 *B* leads to the differential equations of

$$\frac{dE0}{dt} = k_{-1}E1.Cl - k_1[Cl_i]E0, \tag{16}$$

$$\frac{dE1.Cl}{dt} = k_1[Cl_i]E0 + k_{-2}E2.Cl - (k_{-1} + k_2)E1.Cl, \tag{17}$$

$$\frac{dE2.Cl}{dt} = k_2E1.Cl - k_{-2}E2.Cl, \tag{18}$$

where E0, E1.Cl, and E2.Cl are the proportion of prestin in those states, respectively. Since the total amount of prestin is conserved, Eq. 4 gives

$$E_{tot} = E0 + E1.Cl + E2.Cl.$$

In steady state, $dE0/dt = dE1.Cl/dt = dE2.Cl/dt = 0$, so combining Eqs. 16–18 and Eq. 4 gives Eq. 8

$$E2.Cl = \frac{E_{tot}}{1 + \left(\frac{k_{-2}}{k_2}\left(1 + \frac{k_{-1}}{k_1[Cl_i]}\right)\right)}.$$

V_o corresponds to the potential at which the state E2.Cl is half-populated, therefore when $V = V_o$,

$$\frac{k_{-2}}{k_2}\left(1 + \frac{k_{-1}}{k_1[Cl_i]}\right) = 1, \tag{19}$$

$$e^{\frac{\alpha e_o V_o}{k_B T}} = \frac{k_{-2}(0)}{k_2(0)}\left(1 + \frac{k_{-1}}{k_1[Cl_i]}\right), \tag{20}$$

giving Eq. 9,

$$V_o = \frac{k_B T}{\alpha e_o}\ln\left(\frac{k_{-2}(0)}{k_2(0)}\left(1 + \frac{k_{-1}}{k_1[Cl_i]}\right)\right).$$

We thank Dr. Alasdair Gibb for helpful discussion at early stages in this project. This work supported by the Wellcome Trust and the Medical Research Council (UK).

REFERENCES

1. Dallos, P., and D. Harris. 1978. Properties of auditory nerve responses in absence of outer hair cells. *J. Neurophysiol.* 41:365–383.
2. Belyantseva, I. A., H. J. Adler, R. Curi, G. I. Frolenkov, and B. Kachar. 2000. Expression and localization of prestin and the sugar transporter GLUT-5 during development of electromotility in cochlear outer hair cells. *J. Neurosci.* 20:RC116.
3. Liberman, M. C., J. Gao, D. Z. He, X. Wu, S. Jia, and J. Zuo. 2002. Prestin is required for electromotility of the outer hair cell and for the cochlear amplifier. *Nature.* 419:300–304.
4. Ashmore, J. F. 1990. Forward and reverse transduction in the mammalian cochlea. *Neurosci. Res. Suppl.* 12:S39–S50.
5. Santos-Sacchi, J. 1991. Reversible inhibition of voltage-dependent outer hair cell motility and capacitance. *J. Neurosci.* 11:3096–3110.
6. Gale, J. E., and J. F. Ashmore. 1997. The outer hair cell motor in membrane patches. *Pflugers Arch.* 434:267–271.
7. Dallos, P., R. Hallworth, and B. N. Evans. 1993. Theory of electrically driven shape changes of cochlear outer hair cells. *J. Neurophysiol.* 70: 299–323.
8. Iwasa, K. H. 1994. A membrane motor model for the fast motility of the outer hair cell. *J. Acoust. Soc. Am.* 96:2216–2224.
9. Everett, L. A., and E. D. Green. 1999. A family of mammalian anion transporters and their involvement in human genetic diseases. *Hum. Mol. Genet.* 8:1883–1891.
10. Mount, D. B., and M. F. Romero. 2004. The SLC26 gene family of multifunctional anion exchangers. *Pflugers Arch.* 447:710–721.
11. Satoh, H., M. Susaki, C. Shukunami, K. Iyama, T. Negoro, and Y. Hiraki. 1998. Functional analysis of diastrophic dysplasia sulfate transporter. Its involvement in growth regulation of chondrocytes mediated by sulfated proteoglycans. *J. Biol. Chem.* 273: 12307–12315.

12. Scott, D. A., R. Wang, T. M. Kreman, V. C. Sheffield, and L. P. Karniski. 1999. The Pendred syndrome gene encodes a chloride-iodide transport protein. *Nat. Genet.* 21:440–443.

13. Scott, D. A., and L. P. Karniski. 2000. Human pendrin expressed in *Xenopus laevis* oocytes mediates chloride/formate exchange. *Am. J. Physiol. Cell Physiol.* 278:C207–C211.

14. Knauf, F., C. L. Yang, R. B. Thomson, S. A. Mentone, G. Giebisch, and P. S. Aronson. 2001. Identification of a chloride-formate exchanger expressed on the brush border membrane of renal proximal tubule cells. *Proc. Natl. Acad. Sci. USA.* 98:9425–9430.

15. Jiang, Z., I. I. Grichtchenko, W. F. Boron, and P. S. Aronson. 2002. Specificity of anion exchange mediated by mouse Slc26a6. *J. Biol. Chem.* 277:33963–33967.

16. Xie, Q., R. Welch, A. Mercado, M. F. Romero, and D. B. Mount. 2002. Molecular characterization of the murine Slc26a6 anion exchanger: functional comparison with Slc26a1. *Am. J. Physiol. Renal Physiol.* 283:F826–F838.

17. Ko, S. B., N. Shcheynikov, J. Y. Choi, X. Luo, K. Ishibashi, P. J. Thomas, J. Y. Kim, K. H. Kim, M. G. Lee, S. Naruse, and S. Muallem. 2002. A molecular mechanism for aberrant CFTR-dependent HCO_3^- transport in cystic fibrosis. *EMBO J.* 21:5662–5672.

18. Zheng, J., K. B. Long, W. Shen, L. D. Madison, and P. Dallos. 2001. Prestin topology: localization of protein epitopes in relation to the plasma membrane. *Neuroreport.* 12:1929–1935.

19. Oliver, D., D. Z. He, N. Klocker, J. Ludwig, U. Schulte, S. Waldegger, J. P. Ruppersberg, P. Dallos, and B. Fakler. 2001. Intracellular anions as the voltage sensor of prestin, the outer hair cell motor protein. *Science.* 292:2340–2343.

20. Fakler, B., and D. Oliver. 2002. Functional properties of prestin—how the motor molecule works. *In* Biophysics of the Cochlea from Molecules to Models. A.W. Gummer, editor. World Scientific, Singapore. 110–115.

21. Rybalchenko, V., and J. Santos-Sacchi. 2003. Cl- flux through a non-selective, stretch-sensitive conductance influences the outer hair cell motor of the guinea-pig. *J. Physiol.* 547:873–891.

22. Song, L., A. Seeger, and J. Santos-Sacchi. 2005. On membrane motor activity and chloride flux in the outer hair cell: lessons learned from the environmental toxin tributyltin. *Biophys. J.* 88:2350–2362.

23. Lauger, P., and H. J. Apell. 1988. Transient behaviour of the Na^+/K^+-pump: microscopic analysis of nonstationary ion translocation. *Biochim. Biophys. Acta.* 944:451–464.

24. Colquhoun, D., and A. G. Hawkes. 1995. A Q-Matrix Cookbook: How to write only one program to calculate the single-channel and macroscopic predictions for any kinetic mechanism. *In* Single-Channel Recordings. B. Sakmann and E. Neher, editors. Plenum, New York. 589–636.

25. Barry, P. H. 1994. JPCALC, a software package for calculating liquid junction potential corrections in patch-clamp, intracellular, epithelial and bilayer measurements and for correction junction potential measurements. *J. Neurosci. Methods.* 51:107–116.

26. Frank, G., W. Hemmert, and A. W. Gummer. 1999. Limiting dynamics of high-frequency electromechanical transduction of outer hair cells. *Proc. Natl. Acad. Sci. USA.* 96:4420–4425.

27. Marty, A., and E. Neher. 1995. Tight seal whole-cell recordings. *In* Single Channel Recordings. B. Sakmann, and E. Neher, editors. Plenum, New York. 31–52.

28. Ohnishi, S., M. Hara, M. Inoue, T. Yamashita, T. Kumazawa, A. Minato, and C. Inagaki. 1992. Delayed shortening and shrinkage of cochlear outer hair cells. *Am. J. Physiol.* 263:C1088–C1095.

29. Ikeda, K., Y. Saito, A. Nishiyama, and T. Takasaka. 1992. Intracellular pH regulation in isolated cochlear outer hair cells of the guinea-pig. *J. Physiol.* 447:627–648.

30. Kawasaki, E., N. Hattori, E. Miyamoto, T. Yamashita, and C. Inagaki. 1999. Single-cell RT-PCR demonstrates expression of voltage-dependent chloride channels (ClC-1, ClC-2 and ClC-3) in outer hair cells of rat cochlea. *Brain Res.* 838:166–170.

31. Kawasaki, E., N. Hattori, E. Miyamoto, T. Yamashita, and C. Inagaki. 2000. mRNA expression of kidney-specific ClC-K1 chloride channel in single-cell reverse transcription-polymerase chain reaction analysis of outer hair cells of rat cochlea. *Neurosci. Lett.* 290:76–78.

32. Zimmermann, U., I. Kopschall, K. Rohbock, G. J. Bosman, H. P. Zenner, and M. Knipper. 2000. Molecular characterization of anion exchangers in the cochlea. *Mol. Cell. Biochem.* 205:25–37.

33. Cecola, R. P., and R. P. Bobbin. 1992. Lowering extracellular chloride concentration alters outer hair cell shape. *Hear. Res.* 61:65–72.